COMMUNICATION

High-Quality-Factor Mid-Infrared Toroidal Excitation in Folded 3D Metamaterials

Zhe Liu, Shuo Du, Ajuan Cui, Zhancheng Li, Yuancheng Fan, Shuqi Chen, Wuxia Li, Junjie Li,* and Changzhi Gu*

With unusual electromagnetic radiation properties and great application potentials, optical toroidal moments have received increasing interest in recent years. 3D metamaterials composed of split ring resonators with specific orientations in micro-/nanoscale are a perfect choice for toroidal moment realization in optical frequency considering the excellent magnetic confinement and quality factor, which, unfortunately, are currently beyond the reach of existing micro-/nanofabrication techniques. Here, a 3D toroidal metamaterial operating in mid-infrared region constructed by metal patterns and dielectric frameworks is designed, by which high-quality-factor toroidal resonance is observed experimentally. The toroidal dipole excitation is confirmed numerically and further demonstrated by phase analysis. Furthermore, the far-field radiation intensity of the excited toroidal dipoles can be adjusted to be predominant among other multipoles by just tuning the incident angle. The related processing method expands the capability of focused ion beam folding technologies greatly, especially in 3D metamaterial fabrication, showing great flexibility and nanoscale controllability on structure size, position, and orientation.

Toroidal moments are created by poloidal currents or induced magnetic dipoles connecting in a head-to-tail manner.[1] As a class of fundamental electromagnetic excitations, toroidal moments are not represented in conventional multipole expansion, yet are attracting growing interest due to their unusual electromagnetic properties.[2] Although the static toroidal moments have been investigated extensively in various fields such as nuclear, atomic, solid state physics, etc.,[3] the dynamic toroidal moments that have strong interactions with incident light were demonstrated in experiment only recently by metamaterials in microwave region.[4,5] However, a variety of optical functionalities are expected to be realized through dynamic toroidal moments in high frequency region including sensing,[6,7] lasing spaser,[8] and optical force,[9] especially the one with high quality (high-Q) factors.[10,11] Hence in view of its application prospect, lots of efforts are devoted in the extension of the toroidal response frequency into optical region while maintaining high-Q property.

In order to construct dynamic toroidal moments, metamaterial structures are generally used in which a serial of resonant units with same resonance frequency are arranged in such configuration that the magnetic field of each unit can be connected in a head-to-tail way.[4] Among various configurations for toroidal realization, 3D resonance units are preferred[4,12–14] because they offer much better confinement of the circulating magnetic field than their 2D counterparts so that large toroidal dipole intensity and high-Q factor can be obtained. The adoption of vertical split ring resonators (SRRs) is a straightforward route for the realization of toroidal excitations due to the intensively studied magnetic dipoles,[10,11,15] by which the first toroidal moment was demonstrated.[4] Although various kinds of SRR-based toroidal metamaterials have been proposed and successfully fabricated with strong toroidal response in microwave region,[4,6,14] it is hard to extend these 3D structures into micro- or nanoscope for high frequency responses because of the natural limitation of traditional planar micro-/nanofabrication techniques. Persistent effort has also been devoted to other 3D structures including asymmetric double-bar,[16] oligomer of holes,[17] V-groove array,[18] dielectric particles,[19] or cylinders,[20] etc., for toroidal moments in higher frequency region and great progress has been made. However, the magnetic field confinement obtained so far is relatively weak, so that the Q factors are smaller compared to that of the SRR-based metamaterials.[4] As a result, toroidal moment with high-Q factor and a response frequency in optical region is hardly to be realized until a feasible fabrication technique for

**ADVANCED
SCIENCE NEWS**

www.advancedsciencenews.com

**ADVANCED
MATERIALS**

www.advmat.de

COMMUNICATION

micro- and nanosized vertical SRR structures with orientation controllability is developed.

Up to now, a few methods have been developed for the fabrication of vertical SRRs in micro- or nanoscale, such as double exposure e-beam lithographic process,[21] multilayer electroplating,[22] metal stress-driven self-folding method,[23] self-aligned membrane projection lithography,[24] two-photon polymerization process,[25] ion beam induced folding,[26–28] etc., by which the limitation of microfabrication has been pushed to a higher level. However, there remain some challenges encountering us, especially that the split direction and spatial position of each SRR units cannot be controlled at the same time using the state-of-the-art techniques. For example, vertically oriented SRRs with different split directions are successfully fabricated on the sidewall of a dielectric box using membrane projection lithography techniques,[24] yet the split directions of each SRR cannot be changed independently due to the restriction of the patterned membrane; vertical SRRs in controllable spatial position can be easily fabricated by two-photon polymerization process and metal coating,[25] but the open-side-down split ring is not exactly a sole SRR with well excited magnetic resonance because the edge on the bottom side is short-connected by the conductive substrate; focused ion beam has proved to be an effective techniques for 3D micro-/nanostructure fabrication and SRRs with controllable split orientation can be easily obtained,[26–28] whereas, they are located on conductive substrates as well. Therefore, new constructing strategy for 3D micro-/nanostructures is highly needed to explore new 3D metamaterials, especially the one with optical toroidal excitations.

Here, we demonstrated that the adoption of metal patterns on dielectric frameworks can greatly expand the fabrication capability of focused ion beam folding technologies that 3D metamaterials with various configurations can be fabricated in micro-/nanoscale, showing great design flexibility and controllability on size, position, and orientation at the nanometer level. Compared to state-of-the-art techniques, not only the weakness of short-connection between etch unit to the substrate was overcome, but also the diversity of 3D structures can be greatly expanded from just metal structures to various combinations of dielectric and metal. More importantly, a toroidal metamaterial was demonstrated, in which SRRs with different split directions were arranged in 3D configuration using silicon nitride (SiN$_x$) framework. Toroidal resonance was observed in mid-infrared region from transmission measurement showing a high-Q factor. Furthermore, in order to get larger toroidal dipole radiation intensity, oblique excitation was considered, which proves to be a feasible scheme. The 3D structure obtained by this technique is promising to be further scaled down and used in active devices modulated by external mechanical or thermal signals due to the excellent mechanical property of SiN$_x$ film.

Classical metamaterial design, first used for the demonstration of toroidal resonance in microwave region,[4] was adopted to construct 3D metamaterial with toroidal excitation in optical region. Specifically, each toroidal molecule is composed of four SRRs with two of them open-side-up and the other two open-side-down. Here, SiN$_x$ window with low stress suspending SiN$_x$ film, which is both mechanical stable and optical transparent, was used as the upholder of the SRR patterns (**Figure 1**a). After electron beam lithography and metal deposition, Au SRRs were patterned on the SiN$_x$ film (Figure 1b), the scanning electron microscope (SEM) images of which are shown in **Figure 2**a,b. The sample was put up-side-down (Figure 1c) before ion beam processing in order to protect the metal patterns from damaging by the subsequent ion beam scanning (otherwise, the
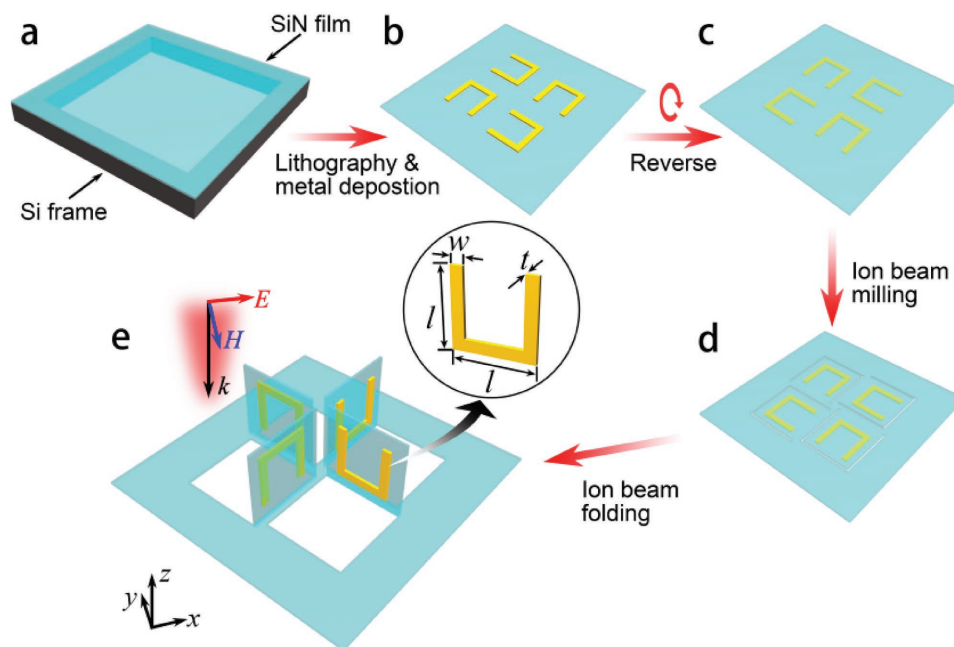

Figure 1. Schematic of fabrication process of the toroidal metamaterial. a) Suspended SiN$_x$ film on silicon frame. b) SRRs on SiN$_x$ film by electron beam lithography and metal deposition process. c) Reversing the film up-side-down. d) Ion beam cutting of SiN$_x$ flakes. e) A toroidal molecule folded by ion beam. The parameters are: l = 1.25 µm, w = 150 nm, t = 80 nm. The side length of the SiN$_x$ flakes is 1.7 µm, and the thickness is 100 nm.
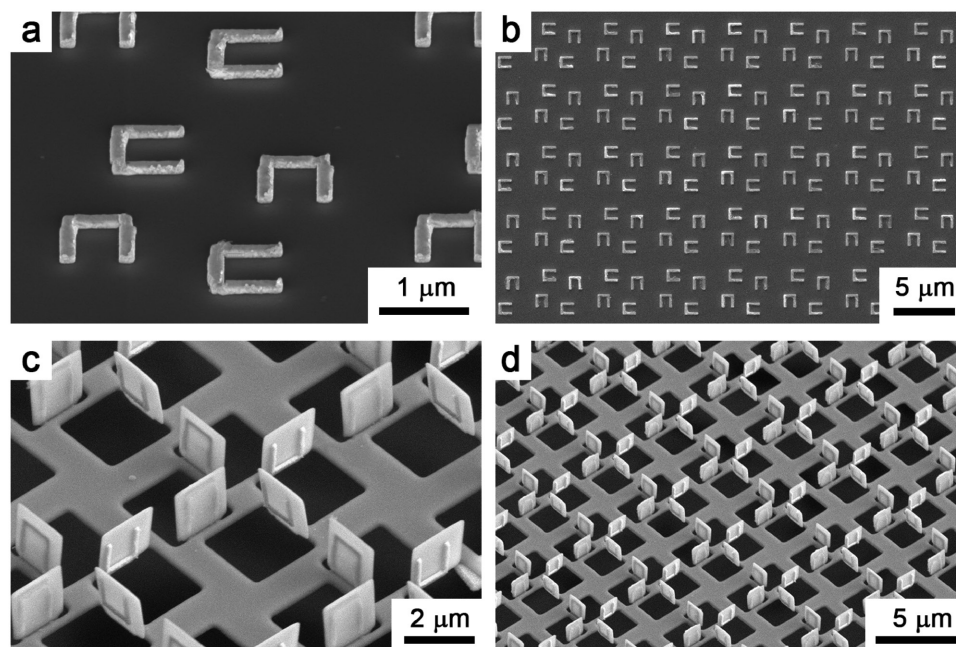
Figure 2. Experimental demonstration of toroidal metamaterials. a,b) SEM images of SRR arrays on planar SiN$_x$ film in 52° tilted view and top view, respectively. c,d) SEM images of toroidal metamaterial array in 52° tilted view.

metal patterns would be damaged as showed in Figure S1 (Supporting Information), which can severely undermine the related optical properties). Focused ion beam was used subsequently to cut the SiN$_x$ film into rectangular flakes a little larger than the SRR patterns, with one end connected to the film (Figure 1d). Finally, focused ion beam induced bending technique[26–28] was used to fold the flakes into designated orientations (Figure 1e). With the above mentioned procedures, this technique possesses lots of advantages: good controllability on the orientation of the SiN$_x$ flakes by controlling ion dose or ion beam direction,[26] nanoscale precision endowed by the focused ion beam spot, high degree of flexibility on 3D construction,[27] and large optionality of materials including dielectric, semiconductor, and metal films. Figure 2c,d shows the SEM images of the as-fabricated toroidal 3D metamaterials that are rectangularly arranged with a period of 5 μm in an array consisting of 20 × 20 units, which is large enough to be measured by a microarea spectroscopic system.

Transmission spectrum is used to study the optical properties of the 3D metamaterial with the incident light illuminating from the positive z direction and the electric component parallel to the x axis (illustrated in Figure 1e), instead of the x direction incidence in the literature.[4,13] The spectra from simulation and measurement are displayed in **Figure 3**a, showing good consistence on peak positions, with the only difference lying in the peak intensity that the measured curve is smaller which can attribute to the structure imperfection of the fabricated sample. Two obvious resonances can be observed in the transmission curve at $\omega_1 = 29.1$ THz and $\omega_2 = 33.6$ THz. The two resonances derive from the hybridization of the two "toroidal atoms"[13] as shown in Figure 3b. The four SRRs in each cell can be divided into two atoms: two SRRs of open-side-down in "atom 1," and two SRRs of open-side-up in "atom 2," and the energy levels

of both "atoms" degenerate and split into two individual resonances.[13] In order to understand the mechanism of the two resonances, the cross-profile of magnetic field on x–y plane in the middle of the toroidal molecule was simulated as shown in Figure 3c,d. As can be seen from Figure 3c, the magnetic field vectors generated by the surface current loop on SRRs was connected in a head-to-tail way at ω_1, demonstrating the existence of a toroidal dipole **T** in z direction. At ω_2, the magnetic field in the four SRRs does not form a loop, instead a vector resultant in the y direction leads to a net magnetic dipole **M**. Thus $\mathbf{T}_z$ dipole and $\mathbf{M}_y$ dipole are excited at ω_1 and ω_2, respectively. Moreover, the Q factors, defined as the ratio of resonance frequency to the full width at half maximum, are 20.78 and 24.96 for ω_1 and ω_2, respectively, extracted from the measured curve (extraction details in Part 2 of the Supporting Information), with a large modulation depth $(1 - \mathbf{T}(\omega_i))$ of about 50%. Compared to our 3D configuration, the 2D toroidal metamaterials usually have much smaller Q factors[29] which is less than 10. Although the Q factors can be improved through a mirrored arrangement of Fano resonators, the modulation depth was sacrificed to be very small,[10] which does not meet the demand of sharp and large resonant intensity in the field of sensing applications.

To further clarify the resonant mechanism of both toroidal and magnetic dipoles, the magnetic fields excited by SRR units at the two resonant frequencies are systematically analyzed. Studies on vertical SRRs show that when there is an electric field component parallel to the bottom of the ring and magnetic field component passing through the rings, both electric and magnetic excitations contribute to the resonance modes.[30] However, when the SRRs have opposite open-side directions (open-side-down and open-side-up), the responses can be excited in different ways. The phase comparison between excited and incident magnetic fields
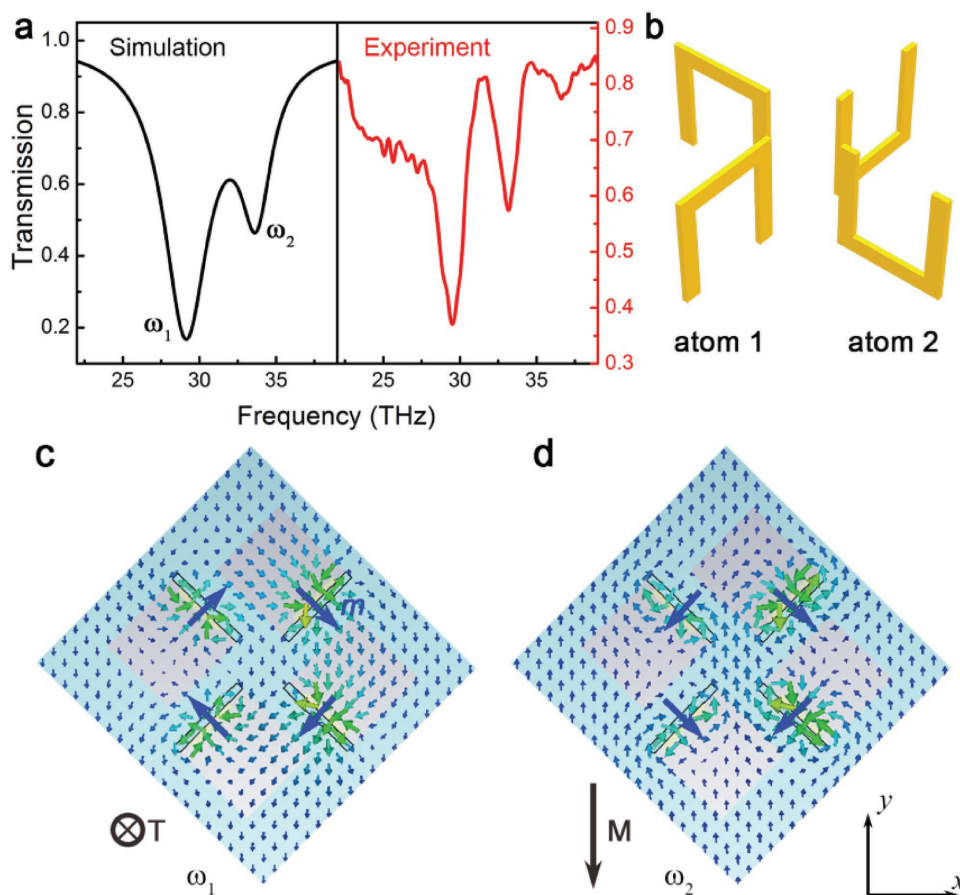
Figure 3. Demonstration of the resonances in 3D metamaterial. a) Transmission spectra of the toroidal metamaterial by simulation and experiment. b) Illustration of toroidal atoms. c,d) Magnetic field distribution at ω_1 and ω_2, respectively.

of both kinds of SRRs (Figure S3, Supporting Information) gives a hint on these differences. For SRR of open-side-down, the excited magnetic field has an opposite direction compared to the incident magnetic field which is accordance with the Lenz's law, while the excited surface current on the bottom side has the same direction with incident electric field, indicating a constructive superposition of the magnetic and electric excitation effects. But for SRR of open-side-up, the excited magnetic field has the same direction with the incident magnetic field, indicating a destructive superposition of the magnetic and electric excitation effects. In short, the two kinds of "atoms" have opposite intrinsic resonance properties.

The combination of two SRRs with opposite split directions has been used to cancel the electric dipole moment in magnetic and negative index metamaterials,[31] and here in this work it also contributes to the excitation of toroidal resonance mode. When there are two kinds of SRRs ("atom 1" and "atom 2") in each molecule, the direction of excited magnetic field should be opposite in the two "atoms." As mentioned previously, the intrinsic resonance of the SRR units split into two resonances, where the excited magnetic fields in the two atoms have the same and different directions at ω_1 and ω_2, respectively. The toroidal resonance at ω_1 is reasonable, considering that the excited magnetic fields with

different directions in "atom 1" and "atom 2" form a loop in a head-to-tail manner, but the resonance at ω_2 should be reconsidered because the excited magnetic fields have the same direction. The intensity and phase of excited magnetic fields in the middle of SRRs are extracted (Figure S4, Supporting Information), which illustrates that at ω_1 the SRR units were synchronously exited, while at ω_2 they were out of sync because the light meet the bottom sides of different SRRs with a phase delay (detailed discussions in Part 4 of the Supporting Information). This means that when light illuminates from z direction, the excitation mechanisms of both toroidal and magnetic responses are different compared to x-direction incidence.[4,13] In addition, simulation results show that a metamolecule composed of SRRs with the same open-side direction has only one magnetic response and no toroidal response (Figure S5, Supporting Information), proving the importance of opposite-split-direction configuration of the four SRRs.

From the above analysis, it can be concluded that it is the excited dipole modes (electric, magnetic, and toroidal) that contribute to the transmission spectra of this toroidal metamaterial, thus the contributions of these dipoles can be quantitatively analyzed by their radiation intensities. The radiation power magnitude of these multipoles can be described as follows[4,13]
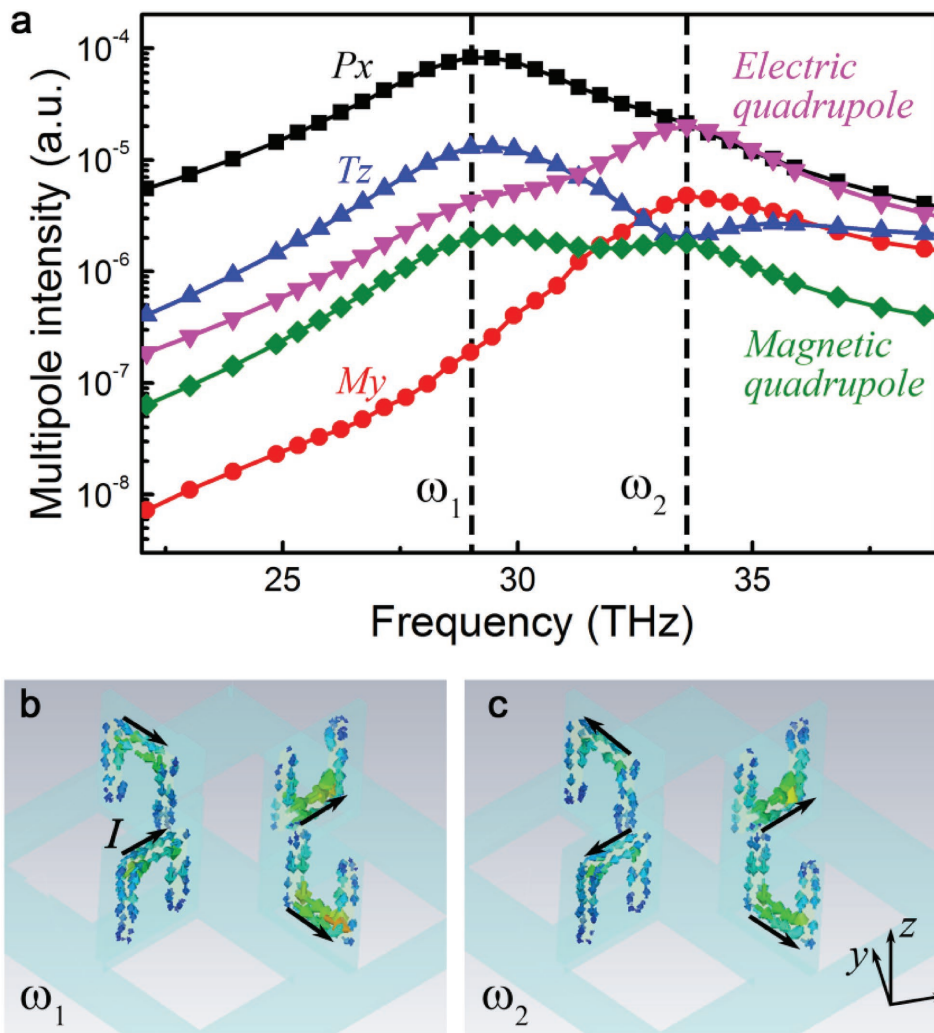
Figure 4. Demonstration of the excited multipoles. a) Dispersion of radiation power for various multipole moments induced in the toroidal metamaterial. b,c) Surface current distribution and electric dipole orientation on SRR units at ω_1 and ω_2.

$$I = \frac{2\omega^4}{3c^3}|\mathbf{P}|^2 + \frac{2\omega^4}{3c^3}|\mathbf{M}|^2$$
$$+ \frac{4\omega^5}{3c^4}|\mathbf{P} \cdot \mathbf{T}| + \frac{2\omega^6}{3c^5}|\mathbf{T}|^2 + \frac{\omega^6}{5c^5}\sum|Q_{\alpha\beta}|^2 \quad (1)$$
$$+ \frac{\omega^6}{40c^5}\sum|M_{\alpha\beta}|^2 + O\left(\frac{1}{c^5}\right)$$

where $\mathbf{P}$, $\mathbf{M}$, $\mathbf{T}$, $Q_{\alpha\beta}$, and $M_{\alpha\beta}$ are the electric dipole, magnetic dipole, toroidal dipole, electric quadrupole, and magnetic quadrupole, respectively, c is the speed of light, ω is the angular frequency, and α, $\beta = x$, y, z. The magnitudes of these multipole moments can be calculated from surface current extracted from simulation (details in Part 6 of the Supporting Information).

The radiation powers as a function of frequency are displayed in **Figure 4**a. Unexpectedly, at ω_1, the x component of the electric dipole $\mathbf{P_x}$ has the largest intensity, which is an order larger than that of the toroidal dipole $\mathbf{T_z}$. The large $\mathbf{P_x}$ comes from the surface current I on the bottom of the SRRs, as shown in Figure 4b. The y components of the current labeled by black arrows on each SRR are cancelled, hence a net vector resultant

along x direction is produced causing large $\mathbf{P_x}$ intensity. This strong $\mathbf{P_x}$ is not desired and should be avoided as much as possible. At ω_2, the strongest multipole moment is not magnetic dipole $\mathbf{M_y}$ but electric quadrupole, of which the current direction on the bottom of SRR can be seen in Figure 3c, and the intensity of $\mathbf{M_y}$ is about one order smaller than the electric quadrupole. This means that in this "toroidal metamaterial," the toroidal moment is not the prominent component due to the strong electric multipoles when the incident light comes from the positive z direction.

So long as the intensity of these multipole components has been fixed, the origin of the transmission minima in Figure 3a can be discussed based on their radiation properties. In general, the transmission of optical signal should be described as $E_{transmitted} = E_{incident} + E_{scattered}$. Here $E_{scattered}$ represents the radiation of the induced multipoles including electric dipole $\mathbf{P_x}$, magnetic dipole $\mathbf{M_y}$, toroidal dipole $\mathbf{T_z}$, and quadrupoles on the SRRs along the direction of wave vector k. Therefore, all the multipoles have contributions to the transmission minimum in the form of out-of-phase cancellation to the incident wave.

**ADVANCED
SCIENCE NEWS**
www.advancedsciencenews.com

**ADVANCED
MATERIALS**
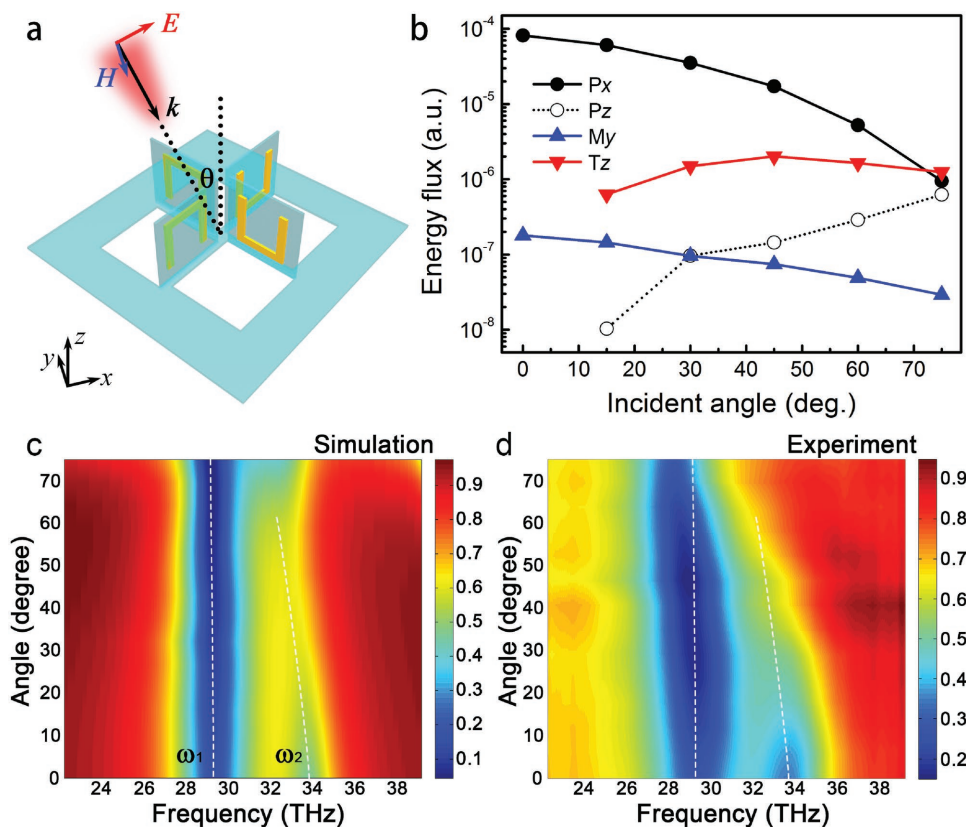www.advmat.de

COMMUNICATION

Figure 5. Far-field radiation property of toroidal metamaterial. a) Schematic of oblique excitation of toroidal resonance. b) Energy flux intensity of different multipole at ω_1 and ω_2. c) Transmission spectra at different incident angles from 0° to 75° by simulation. d) Transmission spectra at different incident angles from 0° to 75° by experiment.

Although the $\mathbf{T}_z$ dipole does not have the largest intensity among all these multipoles, this does not mean that $\mathbf{T}_z$ has the weakest radiation power in the far-field. The energy radiation flux in different directions is not solely related to dipole intensity but also concerned with the radiation angle.[32,33] The far-field radiation pattern of electric dipole can be expressed as[2]

$$\langle S \rangle = \frac{\omega^4}{4\pi c^3} |\mathbf{p}|^2 \left(1 - (\mathbf{r} \cdot \mathbf{p})^2\right) \tag{2}$$

where $\langle S \rangle$ is time-averaged Poynting vector, $\mathbf{r}$ and $\mathbf{p}$ are unit vectors, thus we get

$$\langle S \rangle \propto \sin^2 \theta \tag{3}$$

Here θ is the angle between $\mathbf{r}$ and $\mathbf{p}$ vectors. This relationship is suitable not only for electric dipole, but also for magnetic and toroidal dipoles.[2,32]

Since the incident light comes from z direction, $\mathbf{T}_z$ has no contribution to the far-field radiation power in the forward z direction, while $\mathbf{P}_x$ and $\mathbf{M}_y$ have the largest angular radiation component. This reminds us that if the wave vector k has an angle with respect to z direction, the radiation intensity of $\mathbf{T}_z$ in the direction of k in the far-field will increase while the $\mathbf{P}_x$ will decrease due to the coefficient of $\sin^2\theta$ in Equation (3). **Figure 5**a displays the oblique incidence of p-polarized light,

that the magnetic field is always parallel to the x–y plane. In the far-field of k direction, the radiation flux of $\mathbf{P}_x$, $\mathbf{M}_y$, and $\mathbf{T}_z$ has a coefficient of $\sin^2(\pi/2 - \theta)$, $\sin^2\theta /2$, and $\sin^2\theta$, respectively. Figure 5b shows the normalized energy flux density in k direction at ω_1 when the light incident angle changes from 0° to 75°. The $\mathbf{P}_x$ flux has the largest intensity when θ is 0°, which is also illustrated in Figure 4a. However, when the incident angle increases from 0° to 75°, the $\mathbf{T}_z$ flux increases and the $\mathbf{P}_x$ flux decreases due to different coefficients with respect to angle θ. When the angle reaches 75°, the $\mathbf{T}_z$ flux exceeds $\mathbf{P}_x$ flux, and $\mathbf{T}_z$ has the largest contribution to the macroscopic transmission spectrum. Thus, just by a feasible scheme of adjusting the incident angle, the contribution from the toroidal moments $\mathbf{T}_z$ to the radiation intensity will play a dominate role in the transmission properties of the toroidal metamaterials. It should be noted that in Figure 5b $\mathbf{P}_z$ flux is also given, because it has a coefficient of $\sin^2\theta$, which increases with incident angle. However, its intensity is always smaller than $\mathbf{T}_z$, indicating that $\mathbf{P}_z$ is not the dominant multipole of the macroscopic transmission property.

In order to prove the growing contribution of $\mathbf{T}_z$ to the far-field, further experiments were carried out and the transmission data by oblique incident excitation are shown in Figure 5, which fit very well with the simulated results. From the simulated results in Figure 5c, when the incident angle increases from 0° to 75° with a step of 5°, the modulation depth of

toroidal resonance ω_1 increases from 80% to 97% and move slightly to low frequency (white dashed line), while the Q factor increases by over 70%. The growing Q factor again proves the larger contribution of $\mathbf{T}_z$ at ω_1 compared to $\mathbf{P}_x$. At ω_2, the resonance also shows a red shift as the incident angle increases. The peak shift comes from the phase changes when the incident light reaches "atom 1" and "atom 2" in an oblique way. From the experimental data in Figure 5d, the peak shift of ω_1 is a little larger than the simulated one due to the imperfect sample fabrication and measurement setup. Meanwhile, when the incident angle is very large (over 65°), the modulation depth of ω_1 drops down rapidly. This is because of the reducing projected area of the toroidal metamaterial pattern in the microscope system with a coefficient of $\cos\theta$, and a large proportion of the incident light passes through the SiN$_x$ film instead of interacting with the structures. The magnetic field and surface current distribution at ω_1 with an incident angle of 75° is shown in Figure S6 (Supporting Information), which confirms the existence of toroidal moment.

In conclusion, a fabrication technique for 3D metal–dielectric composite structures in micro-/nanoscale was developed in which dielectric film is used as a framework for ease of the fabrication of metal patterns with arbitrary spatial orientation through focused ion beam induced bending techniques, showing the advantage of good controllability, nanoscale precision, high degree of flexibility on 3D construction, etc., without the weakness of short circuit by conductive substrate. Based on this technique, toroidal metamaterial composed of four SRRs was fabricated, and toroidal moments excited by vertical incident light were observed with high-Q factor in mid-infrared region. The intensity of toroidal dipole in far-field region becomes dominant when the incident angle increases. This technique offers a scalable method for excitation of toroidal moments, which can also be used in other field including 3D optical antennas, light modulators and logic elements, etc.

Experimental Section

Fabrication Process: 5 nm Cr film was first deposited on 100 nm thick SiN$_x$ window (Shanghai NTI Co., Ltd.) as a conductive layer by thermal evaporation, after which polymethyl methacrylate (PMMA) resist (495 A5) was spin-coated on the window and baked at 180 °C for 1 min. Then, the resist layer was patterned with SRR shapes by electron beam lithography (Raith 150). Metal deposition and acetone lift-off process transfers the resist pattern to gold. Focused ion beam (Helios 600i, FEI) was used to cut through the SiN$_x$ film into flakes and then folded them up by scanning the bottom of the flakes from the back side of the SiN$_x$ window. Finally, the Cr conductive layer was removed by wet etching in Ce(NH$_4$)$_4$(NO$_6$)$_6$/CH$_3$COOH solution. It took 2.2 h for the focused ion beam folding fabrication of this 100 × 100 μm pattern using an ion beam current of 0.23 nA. A 3D pattern array with larger area can be fabricated as long as more time is spent, and the time increases proportional to its area. A larger ion beam is also an option to reduce the fabrication time, but it will reduce the fabrication accuracy which leads to bad edges of the SiN$_x$ flakes.

Optical Measurement: Transmission spectra were measured using a ×15, NA (numerical aperture) = 0.4 objective lens in an optical microscope (Hyperion 2000) coupled to a Fourier-transform infrared spectrometer (Vertex 80, Bruker) through a 40 μm × 40 μm spatial aperture. A homemade aperture was inserted between the sample and objective to confine the illumination cone with a conical angle of 5°,

and the samples were tilted correspondingly to obtain normal incidence during measurement.[34] The transmission spectra were calibrated using air (holes of the grid) as a reference.

Numerical Simulation: The transmission spectra were simulated by the finite-difference time-domain method, and the dispersion relation of gold in the simulation was described by Drude model.[35] The current distributions were simulated using the commercial software package CST Microwave Studio. Realistic parameters were used for describing gold's lossy properties, with an electric conductivity of 4.561×10^7 S m^{-1}. The surface current distributions were obtained using an H-field/surface current monitor.

Supporting Information

Supporting Information is available from the Wiley Online Library or from the author.

Acknowledgements

[1] I. B. Zel'dovich, *Sov. Phys. JETP* **1958**, *6*, 1148.

[2] N. Papasimakis, V. A. Fedotov, V. Savinov, T. A. Raybould, N. I. Zheludev, *Nat. Mater.* **2016**, *15*, 263.

[3] a) W. C. Haxton, *Science* **1997**, *275*, 1753; b) V. M. Dubovik, V. V. Tugushev, *Phys. Rep.* **1990**, *187*, 145; c) V. V. Flambaum, D. W. Murray, *Phys. Rev. C* **1997**, *56*, 1641; d) A. Ceulemans, L. F. Chibotaru, P. W. Fowler, *Phys. Rev. Lett.* **1998**, *80*, 1861.

[4] T. Kaelberer, V. A. Fedotov, N. Papasimakis, D. P. Tsai, N. I. Zheludev, *Science* **2010**, *330*, 1510.

[5] N. Papasimakis, V. A. Fedotov, K. Marinov, N. I. Zheludev, *Phys. Rev. Lett.* **2009**, *103*, 093901.

[6] Q. W. Ye, L. Y. Guo, M. H. Li, Y. Liu, B. X. Xiao, H. L. Yang, *Phys. Scr.* **2013**, *88*, 055002.

[7] K. Marinov, A. D. Boardman, V. A. Fedotov, N. Zheludev, *New J. Phys.* **2007**, *9*, 324.

[8] Y.-W. Huang, W. T. Chen, P. C. Wu, V. A. Fedotov, N. I. Zheludev, D. P. Tsai, *Sci. Rep.* **2013**, *3*, 1237.

[9] X.-L. Zhang, S. B. Wang, Z. Lin, H.-B. Sun, C. T. Chan, *Phys. Rev. A* **2015**, *92*, 043804.

[10] M. Gupta, V. Savinov, N. Xu, L. Cong, G. Dayal, S. Wang, W. Zhang, N. I. Zheludev, R. Singh, *Adv. Mater.* **2016**, *28*, 8206.

[11] Y. Fan, Z. Wei, H. Li, H. Chen, C. M. Soukoulis, *Phys. Rev. B* **2013**, *87*, 115417.

[12] V. A. Fedotov, A. V. Rogacheva, V. Savinov, D. P. Tsai, N. I. Zheludev, *Sci. Rep.* **2013**, *3*, 2967.

[13] Y.-W. Huang, W. T. Chen, P. C. Wu, V. Fedotov, V. Savinov, Y. Z. Ho, Y.-F. Chau, N. I. Zheludev, D. P. Tsai, *Opt. Express* **2012**, *20*, 1760.

[14] a) Z.-G. Dong, P. Ni, J. Zhu, X. Yin, X. Zhang, *Opt. Express* **2012**, *20*, 13065; b) L. Guo, M. Li, H. Yang, X. Huang, S. Wu, *J. Phys. D: Appl. Phys.* **2014**, *47*, 415501.

[15] a) N. Katsarakis, T. Koschny, M. Kafesaki, E. N. Economou, C. M. Soukoulis, *Appl. Phys. Lett.* **2004**, *84*, 2943; b) M. Li, L. Guo, J. Dong, H. Yang, *Appl. Phys. Express* **2014**, *7*, 082201; c) T. A. Raybould, V. A. Fedotov, N. Papasimakis, I. Kuprov, I. J. Youngs, W. T. Chen, D. P. Tsai, N. I. Zheludev, *Phys. Rev. B* **2016**, *94*, 035119.

[16] Z.-G. Dong, J. Zhu, J. Rho, J.-Q. Li, C. Lu, X. Yin, X. Zhang, *Appl. Phys. Lett.* **2012**, *101*, 144105.

[17] a) B. Ögüt, N. Talebi, R. Vogelgesang, W. Sigle, P. A. van Aken, *Nano Lett.* **2012**, *12*, 5239; b) N. Talebi, B. Ögüt, W. Sigle, R. Vogelgesang, P. A. van Aken, *Appl. Phys. A: Mater. Sci. Process.* **2014**, *116*, 947.

[18] J. Li, Y. Zhang, R. Jin, Q. Wang, Q. Chen, Z. Dong, *Opt. Lett.* **2014**, *39*, 6683.

[19] a) A. E. Miroshnichenko, A. B. Evlyukhin, Y. F. Yu, R. M. Bakker, A. Chipouline, A. I. Kuznetsov, B. Luk'yanchuk, B. N. Chichkov, Y. S. Kivshar, *Nat. Commun.* **2015**, *6*, 8069; b) W. Liu, J. Shi, B. Lei, H. Hu, A. E. Miroshnichenko, *Opt. Express* **2015**, *23*, 24738; c) W. Liu, J. Zhang, A. E. Miroshnichenko, *Laser Photonics Rev.* **2015**, *9*, 564.

[20] a) A. A. Basharin, M. Kafesaki, E. N. Economou, C. M. Soukoulis, V. A. Fedotov, V. Savinov, N. I. Zheludev, *Phys. Rev. X* **2015**, *5*, 011036; b) J. Li, J. Shao, Y.-H. Wang, M.-J. Zhu, J.-Q. Li, Z.-G. Dong, *Opt. Express* **2015**, *23*, 29138; c) W. Liu, J. Zhang, B. Lei, H. Hu, A. E. Miroshnichenko, *Opt. Lett.* **2015**, *40*, 2293.

[21] W. T. Chen, C. J. Chen, P. C. Wu, S. Sun, L. Zhou, G.-Y. Guo, C. T. Hsiao, K.-Y. Yang, N. I. Zheludev, D. P. Tsai, *Opt. Express* **2011**, *19*, 12837.

[22] K. Fan, A. C. Strikwerda, H. Tao, X. Zhang, R. D. Averitt, *Opt. Express* **2011**, *19*, 12619.

[23] C.-C. Chen, A. Ishikawa, Y.-H. Tang, M.-H. Shiao, D. P. Tsai, T. Tanaka, *Adv. Opt. Mater.* **2015**, *3*, 44.

[24] a) D. B. Burckel, J. R. Wendt, G. A. Ten Eyck, A. R. Ellis, I. Brener, M. B. Sinclair, *Adv. Mater.* **2010**, *22*, 3171; b) D. B. Burckel, J. R. Wendt, G. A. Ten Eyck, J. C. Ginn, A. R. Ellis, I. Brener, M. B. Sinclair, *Adv. Mater.* **2010**, *22*, 5053.

[25] a) X. Xiong, S.-C. Jiang, Y.-H. Hu, R.-W. Peng, M. Wang, *Adv. Mater.* **2013**, *25*, 3994; b) X. Xiong, Z.-H. Xue, C. Meng, S.-C. Jiang, Y.-H. Hu, R.-W. Peng, M. Wang, *Phys. Rev. B* **2013**, *88*, 115105.

[26] A. Cui, Z. Liu, J. Li, T. H. Shen, X. Xia, Z. Li, Z. Gong, H. Li, B. Wang, J. Li, H. Yang, W. Li, C. Gu, *Light: Sci. Appl.* **2015**, *4*, e308.

[27] Z. Liu, A. Cui, Z. Gong, H. Li, X. Xia, T. H. Shen, J. Li, H. Yang, W. Li, C. Gu, *Sci. Rep.* **2016**, *6*, 28764.

[28] Z. Liu, Z. Liu, J. Li, W. Li, J. Li, C. Gu, Z.-Y. Li, *Sci. Rep.* **2016**, *6*, 27817.

[29] a) M. Gupta, R. Singh, *Adv. Opt. Mater.* **2016**, *4*, 2119; b) Y. Bao, X. Zhu, Z. Fang, *Sci. Rep.* **2015**, *5*, 11793.

[30] P. Gay-Balmaz, O. J. F. Martin, *J. Appl. Phys.* **2002**, *92*, 2929.

[31] a) J. B. Pendry, A. J. Holden, D. J. Robbins, W. J. Stewart, *IEEE Trans. Microwave Theory Tech.* **1999**, *47*, 2075; b) D. R. Smith, W. J. Padilla, D. C. Vier, S. C. Nemat-Nasser, S. Schultz, *Phys. Rev. Lett.* **2000**, *84*, 4184; c) R. A. Shelby, D. R. Smith, S. Schultz, *Science* **2001**, *292*, 77.

[32] V. Savinov, V. A. Fedotov, N. I. Zheludev, *Phys. Rev. B* **2014**, *89*, 205112.

[33] E. E. Radescu, G. Vaman, *Phys. Rev. E* **2002**, *65*, 046609.

[34] J. Li, B. Jia, G. Zhou, M. Gu, *Opt. Express* **2006**, *14*, 10740.

[35] A. B. D. A. D. Rakic, J. M. Elazar, M. L. Majewski, *Appl. Opt.* **1998**, *37*, 5271.